Numerical Studies of Magnetohydrostatic Finite-Beta Stellarator Equilibria

F. Herrnegger

Max-Planck-Institut für Plasmaphysik EURATOM-IPP Association, Garching

Z. Naturforsch. **37a**, 879–891 (1982); received March 30, 1982

To Professor Arnulf Schlüter on his 60th Birthday

Properties of finite-beta stellarator equilibria are investigated which are obtained as fully three-dimensional finite-beta solutions of the magnetohydrostatic boundary value problem with the help of the code by Bauer, Betancourt, and Garabedian based on the energy method. In the case of slender $l=2$ stellarator equilibria the displacement of the magnetic axis as well as its helical deformation as functions of beta are found to be close to the known theoretical predictions which were derived for slender low beta $l=2$ configurations of large aspect ratio. In the case of $l=2$ stellarators with moderate aspect ratio the shear has a weak effect on the displacement in contradiction to results from asymptotic theories. A class of $l=0, 1, 2, 3$ configurations with reduced secondary currents could be found showing axis displacements which are at least a factor of three smaller than those in pure $l=2$ stellarators. A critical equilibrium beta value of $\beta_e(0)=0.045$ has been estimated in the W VII-AS stellarator for a bell-shaped pressure profile. Extensive numerical convergence studies are presented.

1. Introduction

In stellarator configurations the displacement of the magnetic axis due to the pressure effect is in leading order linearly proportional to β [1, 2] ($\beta = p/(p + B^2/2)$ = kinetic pressure over the total pressure at the magnetic axis). Limiting the displacement to a fixed fraction of the plasma radius defines a maximum value β_c of beta. This we take as an estimate of the maximum accessible equilibrium value β_e of beta. In the case of an $l=2$ stellarator with a circular magnetic axis the asymptotic theory [1] gives* $\beta_c = 2\iota_0^2/A$; here $A = R_T/b$ is the aspect ratio of the torus related to the mean radius b of the cross-section of the outer conducting wall; ι_0 is the twist number along the full torus at the magnetic axis (angle of rotational transform divided by 2π). This estimate for β_c was derived under the conditions $1/A \ll 1$, $M/A = 2\pi b/L_p \ll 1$; M is the number of field periods around the full torus (so the number N of wire periods is given by $N = M/2$ for an $l=2$ configuration). According to Shafranov [1] the magnetic axis is displaced by an amount of $b/2$ by considering only terms linear in beta if β approaches the value β_c; considering also the nonlinear terms, the displacement is asymptotically limited to $b/\sqrt{3}$ for large values of β/β_c.

Since the shear of an $l=2$ vacuum field is of the order $M/2A$, it can certainly not be neglected when $M \approx A$. Danilkin [3] found for large-shear stellarator fields that the above estimate of the equilibrium value of β is about one order of magnitude too small. In the case of low-β, small-shear $l=2$ configurations the maximum accessible beta value obtained by Danilkin is of the order of that given by Shafranov [1], Greene et al. [2], and that reported here.

Greene et al. [2] showed for $l=2$ stellarators which have a magnetic hill rather than a magnetic well that the outward shift of the plasma column becomes singular at a certain value of β. At this value of β the plasma is marginally stable with respect to an $m=1$, $k=0$ mode (rigid shift). Further estimates of the critical β_c for equilibrium and stability in $l=1$, $l=2$, $l=3$, ... configurations were given by Grad et al. [4] by using various expansion schemes (low β and finite β) and by considering the stability of certain global modes. Mikhailov [5] re-analyzed this problem and discussed the effect of a magnetic well and a magnetic hill. He confirmed the results of [2].

The aim of the present paper is to study the above effects with the help of three-dimensional finite-beta equilibrium solutions of the magnetohydrostatic boundary value problem in a toroidal

* Because of technical reasons ι (jota) instead of ι is printed in the text.

Reprint requests to Dr. U. Schumacher, Max-Planck-Institut für Plasmaphysik, D-8046 Garching.

0340-4811 / 82 / 0800-0879 $ 01.30/0. — Please order a reprint rather than making your own copy.

domain. While analytical methods (e.g. [1, 6]) and several fully three-dimensional codes (e.g. [7, 8, 9]) (with no other approximations than that of the finite grid size) are available, the code by Bauer, Betancourt, and Garabedian [7] (denoted by BBG code in the following) turned out to be an especially versatile tool and is used here. In Sect. 2 the coordinate system, the boundary conditions, and the choice of the invariant functions (rotational transform and mass distribution as functions of the magnetic surfaces) are described. Numerical convergence studies (to zero mesh size) for the energy, and both the average displacement and the helical $l=1$ deformation of the magnetic axis in $l=2$, $l=1, 2$ stellarators, and $l=0, 1, 2, 3$ configurations are performed in Sects. 3 and 4. The dependence of the axis displacement and the helical deformation of the magnetic axis on β is given in Sect. 3 for $l=2$ and in Sect. 4 for more general $l=0, 1, 2, 3$ stellarator configurations, and is compared with analytical results.

The equilibrium computations are performed over one field period of length L_p. Detailed stability investigations of these equilibria are beyond the scope of this paper. However possible instabilities, saturation phenomena, and interaction of unstable modes obeying the same toroidal periodicity conditions (in particular the rigid radial disturbance corresponding to an $m=1$, $k=0$ mode) are inherently studied as well. The parameter studies (beta variation) of the equilibrium computations are performed in such a way that the rotational transform (twist number ι) as function of the labeling coordinate s is prescribed in a given configuration and the β-value is changed from case to case by changing an s-independent factor in the mass function.

The iteration procedure to minimize the potential energy is continued until typically about seven decimal figures of the potential energy remain constant.

A comparison of results on high-β, $l=0$, 1, 2 stellarator equilibrium computations, including a vacuum field outside the plasma, with the ISAR T1-B experiment [10] was made by Herrnegger et al. [11]. A synopsis of results with the BBG code (further finite-beta results in advanced stellarators with reduced Pfirsch-Schlüter currents are reported in [12, 13]) and the Chodura-Schlüter code [8] is given in [14].

2. Boundary Conditions and Choice of Invariant Functions

2.1. Coordinate System

The coordinate system is shown in Figure 1. The transformations from Cartesian coordinates (x, y, z) to orthogonal modified cylindrical coordinates (r, θ, z) having the origin at R_T are defined by

$$x = (R_T + r)\cos\theta\,, \qquad y = (R_T + r)\sin\theta\,, \quad z = z\,. \tag{1}$$

The plasma is surrounded by an ideally electrically conducting wall which is a magnetic surface. A new coordinate system (s, u, v) is introduced in the plasma region tied to the equilibrium magnetic surfaces, the origin of which is at the magnetic axis. A set of nested toroidal flux surfaces is assumed each of which is used as Lagrangian coordinate surface and labelled by s; s has the value $s=0$ at the magnetic axis and the value $s=1$ at the outer conducting wall. The coordinate v varies in the range $0 \leqq v \leqq 1$ and is related to the toroidal angle θ by $\theta = 2\pi v/M$, where M is the number of field periods around the torus.

The full torus consists of M equal sectors and is passed once for $0 \leqq \theta \leqq 2\pi$. The length L_P of a field period is measured along the circle with the torus radius R_T and is given by $L_P = 2\pi R_T/M$. The relation between the toroidal aspect ratio A, the helical aspect ratio A_h, and M is given by $A_h = L_P/2\pi b = A/M$ ($\varepsilon = 2\pi b/L_P$ is the periodicity number of the field period). The coordinate u ($0 \leqq u \leqq 1$) parameterizes the poloidal angle in meridional planes.

The magnetic axis has the parameter representation $r_a(v)$, $z_a(v)$. The dimensionless radius function $R(s, u, v)$ is related to r and z by the equations

$$r = r_a(v) + R(s, u, v)\,[r_b(u, v) - r_a(v)]\,, \qquad z = z_a(v) + R(s, u, v)\,[z_b(u, v) - z_a(v)]\,, \tag{2}$$

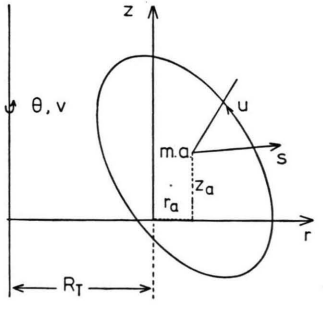

Fig. 1. Coordinate system.

where $r_b(u, v)$, $z_b(u, v)$ is the parameter representation of the outer conducting wall. As an initial condition, R is taken to be a function of s only: $R^2 = s(1+cs)/(1+c)$; here c can be chosen arbitrarily; typical values are $c = 0, 2, 4$ for the following study.

The shape of the outer conducting wall was in the earlier part of this work represented by

$$\begin{aligned} r_b(u,v)/b &= \varrho_b \cos U + \Delta_1(1-\alpha)\cos V \\ &\quad - \Delta_2 \cos(U-V), \\ z_b(u,v)/b &= \varrho_b \sin U + \Delta_1(1+\alpha)\sin V \\ &\quad + \Delta_2 \sin(U-V), \end{aligned} \tag{3}$$

where $U = 2\pi u$, $V = 2\pi v$,

$$\begin{aligned} \varrho_b(u,v) = 1 &- \Delta_0 \cos V + \sum_{l=1,2,\ldots} \Delta_{l0} \cos lU \\ &- \sum_{l=3,4,\ldots} \Delta_l \cos(lU - V) \\ &+ \sum_{l=2,3,\ldots} \sum_{m=2,3,\ldots} \Delta_{lm} \cos(lU - mV). \end{aligned} \tag{4}$$

A modified boundary representation avoiding the formation of trefoils at larger amplitudes of the corrugations has been found to be more advantageous [13] and is given in the figure caption of Figure 17.

The helical $l = 0, 1, 2, \ldots$ corrugations corresponding to the dimensionless amplitudes Δ_l are periodic in v with the period unity (corresponding to the period length L_P). In particular, the Δ_2-deformation of the boundary is an exact ellipse in the planes $v =$ constant; they revolve uniformly around their geometric centre if v is increased from zero to one. The relation between their half-axis ratio e and the ellipticity Δ_2 is given by $\Delta_2 = (1-e)/(1+e)$. The period of the helical corrugations corresponding to Δ_{lm} is given by $1/m$ (corresponding to the length L_P/m); Δ_3 and Δ_{32} describe helical $l = 3$ corrugations which revolve by an angle of $2\pi/3$ and $4\pi/3$, respectively, per field period length L_P. Axisymmetric corrugations are denoted by Δ_{l0} $(l = 1, 2, \ldots)$.

The geometric centre of the cross-sections moves on a toroidal helix-like curve wound on a torus of elliptical cross-section with half-axes $(1-\alpha)\Delta_1$ and $(1+\alpha)\Delta_1$. The deviation from a circular torus is described by α; at $\alpha = -1$ the helicoidal line degenerates to a plane, non-circular toroidal curve oscillating around the circle of given radius $R_T + \Delta_{10}$. The sign of the corrugation Δ_1 is chosen such that at $v = 0$ (standing ellipse for $\Delta_2 > 0$) the helical curve of the geometric centre of the boundary contours starts at the outer edge of the torus for $\Delta_1 > 0$ and at the inner edge for $\Delta_1 < 0$.

The "bumpiness" of the configuration with period length L_P is denoted by Δ_0; it describes the ratio of the cross-sectional area at $v = 0$ and $v = 1/2$; $\Delta_0 > 0$ means that the area at $v = 0$ is smaller than that at $v = 1/2$.

The twist number of the vacuum field associated with these corrugations may be approximately calculated by means of (6) (see below).

2.2. *Twist, Shear, Pressure Profile*

Two invariant functions depending on s are to be prescribed, namely the twist number $\iota(s)$ and the mass $m_s(s)$ within a magnetic surface. The invariant mass function is determined by prescribing an initial pressure distribution $p(s)$ and assuming throughout $p = \varrho_s^2$. The mass density $\varrho_s(s)$ and the computed initial volume $\mathcal{V}(s)$ define then $m_s(s)$.

The initial profile of the twist number per field period, ι_P, is represented as a power series in the radius function R:

$$\begin{aligned} \iota_P &= \mu_0 + \mu_2 R^2 + \mu_4 R^4 + \mu_6 R^6 + \cdots; \\ \iota &= M \iota_P. \end{aligned} \tag{5}$$

In order to give approximately the twist number ι_P of toroidal vacuum fields associated with the given corrugations of the wall, the coefficients of (5) are found either from the corresponding analytical formulas for straight, helically symmetric vacuum fields, (6), or are determined by a fit to the actual ι-profile of the toroidal vacuum field whose outermost magnetic surface is approximated (see, for example, Section 3.3). The applied analytical formulas for the twist number ι_P for vacuum stellarator fields were derived from [1] and read

$$\begin{aligned} \iota_P = \sum_{n=1,2,\ldots} n \left[\frac{b_n}{B_0}\left(\frac{n}{2}\right)^n \frac{1}{n!}\right]^2 \Bigg\{ &\left(1 - \frac{1}{n}\right)\varrho_n^{2n-4} \\ &+ \frac{n}{2}\varrho_n^{2n-2} + \frac{n^2(2n+3)}{4^2(n+1)}\varrho_n^{2n} + \frac{n^4}{3\cdot 4^3(n+1)} \\ &\cdot \left(1 + \frac{3(n+3)}{n+1}\right)\varrho_n^{2n+2} + \frac{n^6}{4^4(n+1)(n+2)} \\ &\cdot \left[\frac{(n+3)(n+4)}{4(n+1)(n+2)} + \frac{1}{12} + \frac{(n+4)}{(n+1)}\right]\varrho_n^{2n+4} + \cdots \Bigg\}, \end{aligned} \tag{6}$$

where $\varrho_n = \varepsilon\varrho/n$, $\varepsilon = 2\pi b/L_P$; ϱ is the minor dimensionless mean radius of a magnetic surface; b_n/B_0 measures the amplitude of the helical fields related to the main magnetic field B_0. In the case of a single helical field the twist number per wire period is $\iota_{WP} = n\iota_P$, since the wire period is n times the field period. A few terms are given explicitly in terms of the corrugations $\Delta_{l\,ax}$ on axis*:

$$l=1:\ \iota_{P1} = \frac{1}{2}(\varepsilon\Delta_{1ax})^2 \cdot\left[1+\frac{5}{16}(\varepsilon\varrho)^2+\frac{7}{192}(\varepsilon\varrho)^4+\frac{41}{9216}(\varepsilon\varrho)^6+\cdots\right], \tag{7a}$$

$$l=2:\ \iota_{P2} = \Delta_{2ax}^2 \cdot\left[1+\frac{1}{2}(\varepsilon\varrho)^2+\frac{7}{96}(\varepsilon\varrho)^4+\frac{1}{192}(\varepsilon\varrho)^6+\cdots\right], \tag{7b}$$

$$l=3:\ \iota_{P3} = 2(\Delta_{3ax}\varrho)^2 \cdot\left[1+\frac{1}{4}(\varepsilon\varrho)^2+\frac{3}{128}(\varepsilon\varrho)^4+\cdots\right], \tag{7c}$$

where

$$b_1/B_0 = 2\varepsilon\Delta_{1ax},\quad b_2/B_0 = 2\Delta_{2ax},$$
$$3b_3/8B_0 = 2\Delta_{3ax}/\varepsilon,$$
$$2b_4/3B_0 = \Delta_{4ax}/\varepsilon^2,\quad \varrho = R.$$

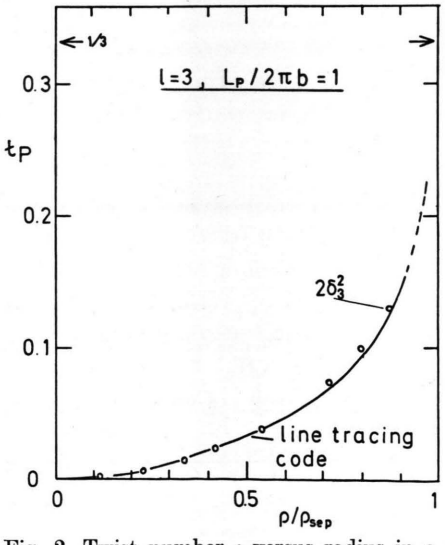

Fig. 2. Twist number ι versus radius in a straight $l=3$ vacuum field.

* At larger values of the $l=2$ deformation Δ_2 (which is the leading deformation in the following applications) the twist number ι_{P2} was approximately calculated by $\Delta_2^2/(1+\Delta_2^2)$ which is accurate to $0(\Delta_2^4)$ in the deformation.

In leading orders in ϱ and Δ_l the twist number of helical vacuum fields with the field period L_P is approximately given by $\iota_{Pl} = (l-1)\Delta_l^2\varrho^{2(l-2)}$, where for the moment Δ_l is the corrugation of the magnetic surfaces at the radius ϱ. Since these formulas are applied later to compute nearly current-free equilibria, the agreement (see Fig. 2) between these estimates and the numerically calculated rotational transform was checked for a straight helical $l=3$ field with a rather large corrugation by using a field-line-tracing code; Fig. 3 shows the contours of the magnetic surfaces for $L_P/2\pi b = 1$, $\delta_3 := \Delta_3\varrho$. Analogous studies were done for $l = 1, 2, \ldots$ fields.

Analytical estimates for the relative depth of the magnetic well depending on these parameters are given in, for example, [1, 15] for systems with a circular magnetic axis (according to [1], p. 183, the depth of the magnetic well in a slender $l=2$ configuration is given by

$$[11/2 - \Delta_2{}^2 M^2/(1+\Delta_2{}^2)^2]/\{A^2[1-4\Delta_2{}^2/(1+\Delta_2{}^2)^2]^{1/2}\} > 0)$$

and in, for example, [1, 16] for systems with a spatial magnetic axis.

The initial distribution of the pressure p is a modified Gauss function

$$p = p_0[\exp(-\sigma R^2) - \exp(-\sigma)]/[1-\exp(-\sigma)]$$

(see Fig. 4), where σ defines the compression ratio $\varkappa = b/a$; the mean plasma radius a is measured

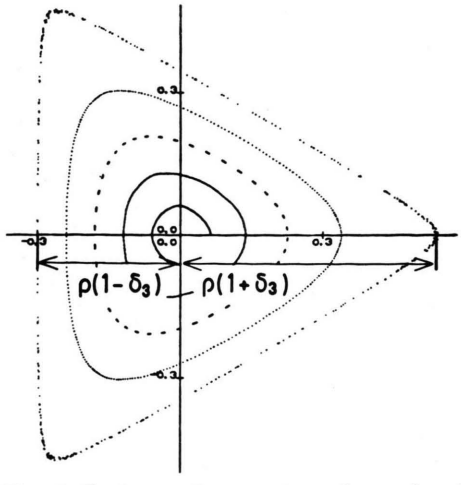

Fig. 3. Contours of magnetic surfaces of a straight $l=3$ vacuum field ($L_P/2\pi b = 1$).

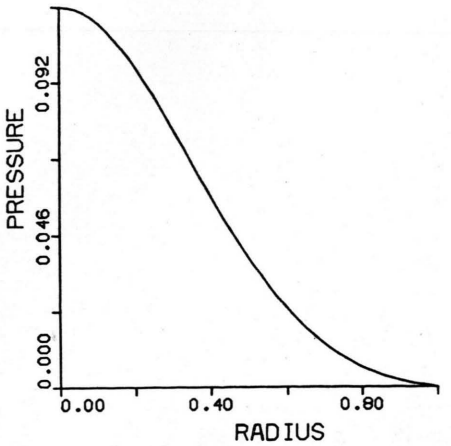

Fig. 4. Pressure profile:
$p = p_0[\exp(-\sigma R^2) - \exp(-\sigma)]/[1 - \exp(-\sigma)]$, $\sigma = 4$.

where the pressure has the $\exp(-1)$-fold value of the maximum pressure p_0. Typical values are $\varkappa = 2$ ($\sigma = 4$), $\varkappa = 1.7$ ($\sigma = 2$), $\varkappa = 1.3$ ($\sigma = 0.5$). Throughout this paper $\varkappa = 2$ is used if not stated otherwise. In case of $\sigma = 4$ and low β the mean $\langle\beta\rangle$-value averaged over the volume is approximately $\langle\beta\rangle = \beta/4$ of the maximum β-value at the magnetic axis.

3. Numerical Convergence Studies, Results on $l = 2$ Stellarators

Convergence studies for the potential energy $W = \iiint_{\mathcal{V}} (p + B^2/2)\, \mathrm{d}\mathcal{V}$ ($\mathcal{V}$ is the plasma volume), the axis shift ξ, and the helical $l = 1$ deformation of the magnetic axis with mesh size will be reported. In the following the distance between the mean position of the magnetic axis and the mean geometric centre of the outer wall is called axis shift ξ. The distance between the mean position of the magnetic axis in finite-β configurations and the mean position of the magnetic axis of the corresponding $\beta = 0$ configuration (vacuum field) is called axis displacement δ and is given by $\delta = \xi(\beta) - \xi(0)$, where $\xi(0)$ is the axis shift for $\beta = 0$. The analytically calculated axis displacement of [1, 2, 17] will be compared with the numerical results.

3.1. Convergence of Energy with Mesh Size

Because the physical quantities strongly depend on the discretization errors in three-dimensional computations and because the computer time and storage are limited, extensive numerical convergence studies are required. Relevant results can only be obtained by a convergence study in the grid size. The discretization of the problem was performed on an equally spaced grid of mesh sizes Δs, Δu, Δv. The convergence studies were carried out by varying the mesh sizes simultaneously at constant ratios $\Delta s : \Delta u : \Delta v$ which define a certain straight line through the origin in the $(\Delta s, \Delta u, \Delta v)$ parameter space, and, in some cases, by varying each mesh size separately. The dependence of the convergence rate on the mesh size is different in the various directions of the parameter space $(\Delta s, \Delta u, \Delta v)$ and also depends on the physical parameters.

On a given straight line of convergence through the origin in the $(\Delta s, \Delta u, \Delta v)$-space the potential energy W is represented according to Ref. [18] as a power series in Δs:

$$W(\Delta s) = W_0 + W_2(\Delta s)^2 + W_\nu(\Delta s)^\nu + W_4(\Delta s)^4 + \cdots . \tag{8}$$

In the particular case of W VII-A parameters the extrapolated value W_0 and the coefficients W_i of Eq. (8) are determined by solving a weighted least squares approximation problem and read as follows (g is the weight function; the numbers of intervals in s, u, v directions, NS/NU/NV, are varied from 10/10/20 to 30/30/60, $c = 4$, $\beta = 2 \cdot 10^{-4}$):

W_0	W_2	W_ν	W_4	g	ν
45.11252	38.82			$1/(\Delta s)^2$	—
45.11124	41.12	— 6.72	— 53.97	1	5/2
45.11128	40.97	— 6.07	— 61.10	$1/(\Delta s)^2$	5/2
45.11131	40.37	— 17.58	— 16.31	1	3
45.11134	40.32	— 16.27	— 24.61	$1/(\Delta s)^2$	3

Instead of calculating the extrapolated value W_0 by means of least-squares approximations (8), a local quadratic polynomial $W_0 + W_2 x^2$ ($x := \Delta s$ for the moment) was fitted through two neighbouring points x_i, x_{i+1}. The value of W_0 then depends on the location of the interval (x_i, x_{i+1}). This series of numbers $W_0(x_i)$ was extrapolated for $x \to 0$ and gives $W_0 = 45.1113$. All the extrapolated values for W_0, which have been determined by means of a polynomial of degree higher than two lie within a relative deviation of the order $1 \cdot 10^{-6}$ which is in the order of the accepted accuracy for the energy as obtained by the iteration procedure of the BBG code.

The same procedures have been applied to determine the extrapolated energy W_0 in a low-β, straight $l=2$ stellarator equilibrium ($\beta=0.004$, $\Delta_2=0.333$, $1/\varepsilon=2.83$, $\iota_P=0.09395+0.00587\,R^2$) with a bell-shaped pressure profile $p=p_0\,(1-R^2)^2$. The iteration procedure to minimize the potential energy is continued until about ten decimal figures remain constant. The effect of the discretization error in simple, straight, helical configurations is substantially smaller than in toroidal configurations. As a result the coefficients W_i ($i=2,\ldots$) of the polynomial (8) are typically three orders of magnitude smaller than in the toroidal $l=2$ configuration and read as follows ($c=0$; up to 45/36/36 grid):

W_0	W_2	W_3	W_4	g	ν
31.60753111	0.03318	−0.00044	−0.6609	1	5/2
31.60753112	0.03314	−0.00150	−0.6539	1	3

The extrapolated value of the energy is found to be $W_0=31.6075311$ with all three above mentioned extrapolation methods and lies within a relative deviation of about $3\cdot10^{-8}$. This result was compared [19] with W_0 (TUBE) $=31.6075328$, which is computed with the TUBE code; they agree within a relative deviation of about $1\cdot10^{-7}$. In this case, comparison of convergence studies for the potential energy with different values of the parameter c ($c=4, 2, 0$) showed that for $c=0$ the convergence rate is more than two orders of magnitude faster than in the case $c=4$, i.e. in leading order $W_2(c=0)/W_2(c=4)\approx 2\cdot10^{-3}$.

3.2. Toroidal $l=2$ Configurations with Small Shear

In the following the W VII-A stellarator configuration ($M=5$) is simulated. This is an $l=2$ configuration of large toroidal and fairly large helical aspect ratio: $A=20$, $A/M=4$. Because of the large helical aspect ratio the shear is small. The single wall parameter used is the elliptical deformation $\Delta_2=0.35$ ($\Delta_{2ax}=0.34$). The spatial dependence of ι is approximately given according to (7b),

$$[5\Delta_{2ax}^2/(1+\Delta_{2ax}^2)\approx 0.53,\ 0.53\,\varepsilon^2/2\approx 0.02],$$

by $\iota=0.53+0.02\,R^2$, which is in close agreement with the ι-profile obtained from vacuum fields by a field-line-tracing code; $\beta_c=2\iota_0^2/A=0.028$; ι_0 and ι_b are the values of ι around the torus at the magnetic axis and at the boundary, respectively; the magnetic well is about 1% according to Shafranov's relation (see Section 2.2). Figure 5 shows the flux surface contours of this stellarator configuration for $\beta=0.022$ (obtained with compression ratio $\varkappa=2$) at three different meridional planes $v=0$, $v=1/4$, $v=1/2$. In Fig. 6 the axis shift ξ is plotted as a function of the mesh size Δs and for various values of β.

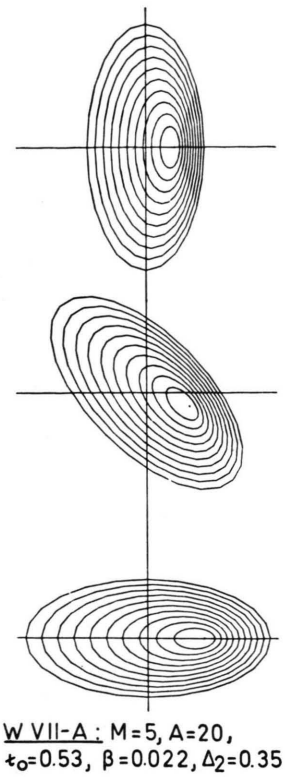

Fig. 5. Finite-β flux surface contours of the $l=2$ stellarator W VII-A: $A=20$, $M=5$, $\Delta_2=0.35$, $\iota_0=0.53$, $\iota_b=0.55$, $\beta=0.022$ ($\langle\beta\rangle=0.006$) (Gaussian pressure profile with $\varkappa=2$).

Because of the torus effect the axis shift ξ is not zero at $\beta=0$ (vacuum case). The approximate analytical value of ξ_V in vacuum stellarator configurations is given for $M/A\ll1$ according to [1] by

$$\xi_V=\frac{1}{A}\left[1-\frac{1}{4l}\right]\Big/\left[l-1+\frac{1}{2}\left(\frac{M}{A}\right)^2\right], \qquad (9)$$

which gives $\xi_V=0.04$ (marked by an arrow in Fig. 6) for $l=2$, $A=20$, $M=5$. The extrapolated value determined numerically corresponds well to the analytical value.

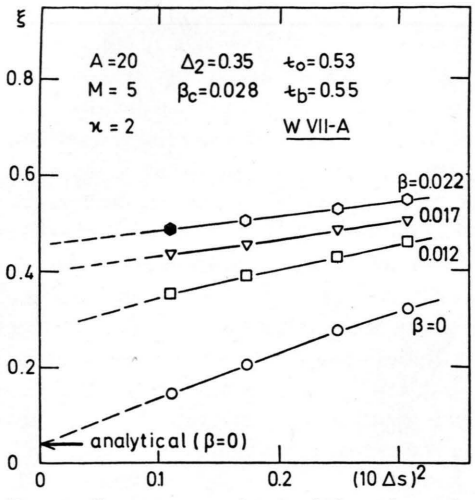

Fig. 6. Convergence of axis shift with mesh size in the W VII-A stellarator for several β-values. The finest grid is NS/NU/NV = 30/30/60.

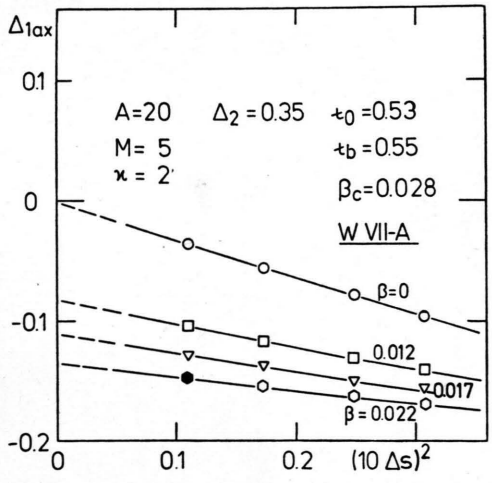

Fig. 7. Convergence of helical $l=1$ deformation Δ_{1ax} of the magnetic axis with mesh size in the W VII-AS stellarator for several β-values (same grids as in Figure 6).

In finite-β configurations a helical $l=1$ corrugation of the magnetic surfaces appears [15] besides the axis shift ξ although the boundary has no $l=1$ corrugation. The helical $l=1$ deformation of the axis is denoted by Δ_{1ax} and is plotted in Fig. 7 as a function of Δs at various values of β. In the case $\beta=0$ ($l=2$ vacuum field) the extrapolated value of Δ_{1ax} vanishes in accordance with asymptotic analytical results [15] and numerical vacuum field computations by a field-line-tracing code. As the plasma pressure increases, the helical $l=1$ deformation of magnetic surfaces increases with the maximum value at the axis. The period length of this deformation coincides with L_P.

Relative to the $l=2$ corrugation ($\Delta_2>0$) the phase of the $l=1$ corrugation is such that at $v=0$ the magnetic axis is moved closer to the inner edge of the torus (radially inward shift in the plane of standing ellipse), and that at $v=1/2$ the magnetic axis is moved closer to the outer edge of the torus (i.e. radially outward shift in the plane of lying ellipse; see Fig. 5); this phase corresponds to $\Delta_{1ax}<0$. Consequently, the helical $l=1$ corrugation of period L_P with $\Delta_1>0$ can be used to diminish the helical deformation of the plasma column. Results are shown in Fig. 8 for W VII-A parameters. Here the axis displacement δ (solid curve) and the helical $l=1$ deformation Δ_{1ax} at the magnetic axis (dashed curves) are plotted versus β/β_c for two different helical corrugations of the wall. The case with $\Delta_1=0$ represents the extrapolated values of the axis displacement in the W VII-A stellarator as discussed above. In the other case the wall has a small helical corrugation $\Delta_1=0.1$, which shifts the plasma by a small amount to the

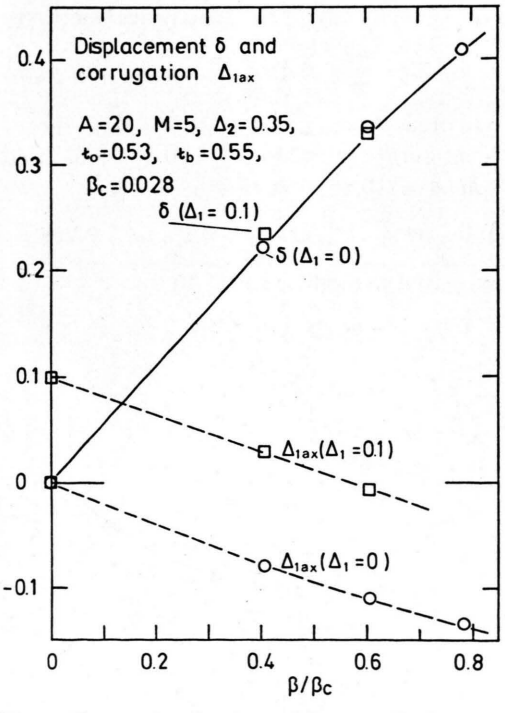

Fig. 8. Extrapolated values of the axis displacement δ and the helical axis deformation Δ_{1ax} versus β/β_c in $l=2$ and $l=1$, 2 stellarators.

main torus axis (i.e. the axis shift of the vacuum field is reduced).

At $\beta=0$ the $l=1$ deformations of the wall and of the magnetic axis are about the same. Accordingly the rotational transform due to the $l=1$ field is almost uniform in accordance with (7a). The twist number around the torus associated with the $l=1$ deformation $\Delta_1=0.1$ is approximately $(\Delta_1 M/A)^2 M/2 \approx 1.6 \cdot 10^{-3}$ and consequently very small compared to $\iota_0=0.53$. Therefore the effect of the $l=1$ field on the shift will be small. Increasing β, the $l=1$ deformation of the axis becomes smaller than that of the wall, so that the effect of the $l=1$ corrugation on the axis shift diminishes. Increasing the β-value further the phase of the $l=1$ deformation of the axis becomes opposite to that of the boundary. Thus a small helical $l=1$ corrugation of the boundary with appropriate phase and β-dependent amplitude eliminates the helical deformation Δ_{1ax} of the axis. This is shown in Fig. 8 (in this case Δ_{1ax} vanishes at $\beta/\beta_c \approx 0.6$). This result is different from that reported in [20] where it is conjectured that the spiralling can only be removed by a vertical field. Finite-β, $l=2$ stellarators with a circular magnetic axis are discussed in, for example, [21] by asymptotic analytical methods.

3.3. *Short Pitch $l=2,4$ Configurations of Large Shear*

The vacuum twist number of a large shear $l=2,4$ configuration with $M=10$ periods and $A=7.7$ ($M/A=1.3$, $\Delta_2=0.25$, $\Delta_{2ax}=0.17$,

$$10\,\Delta_{2ax}^2/(1+\Delta_{2ax}^2) \approx \iota_0 = 0.28,\ \iota_b = 0.79)$$

is approximated according to (6) by

$$\iota = 0.28 + 0.16\,R^2 + 0.35\,R^4.$$

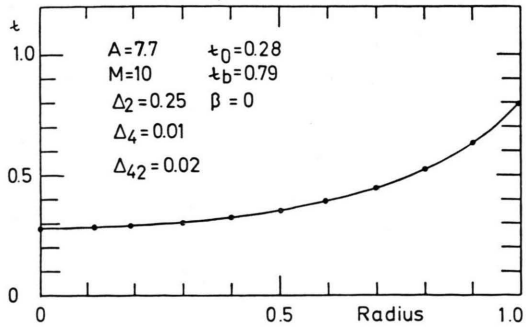

Fig. 9. Twist number versus mean radius of the magnetic surfaces for a short pitch $l=2,4$ stellarator.

In Fig. 9 ι is plotted as a function of the mean radius of the flux surface contours (solid curve). The twist number as obtained by tracing the vacuum magnetic field lines (dots) coincides well with the solid curve. The flux surface contours obtained from the finite-β equilibrium computations made with the BBG code are shown in Fig. 10 and compared in [14] with the magnetic surfaces as obtained by field line tracing. In Fig. 11 the shift ξ and the helical $l=1$ deformation Δ_{1ax} on axis are given for several values of β. A strong dependence of the shift on β can be observed. In numerical simulations, at β-values of $\beta \gtrsim 0.052$ the plasma column drifted in the radial outward direction and no numerical convergence was achieved, whereas at $\beta=0.035$ the convergence is quite good.

Comparing the axis displacement of the plasma in this large-shear $l=2$ configuration with the result in the slender small-shear $l=2$ configuration W VII-A (see Sect. 3.2), it may be concluded that

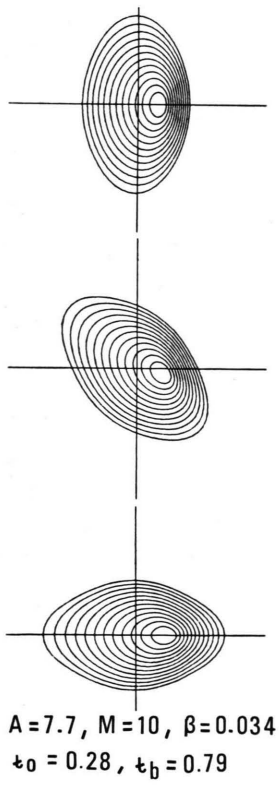

Fig. 10. Flux surface contours of a short pitch $l=2,4$ stellarator: $A=7.7$, $M=10$, $\Delta_2=0.25$, $\Delta_4=0.01$, $\Delta_{42}=0.02$, $\iota_0=0.28$, $\iota_b=0.79$, $\beta=0.035$, $\beta_c=0.02$, NS/NU/NV = 24/48/48.

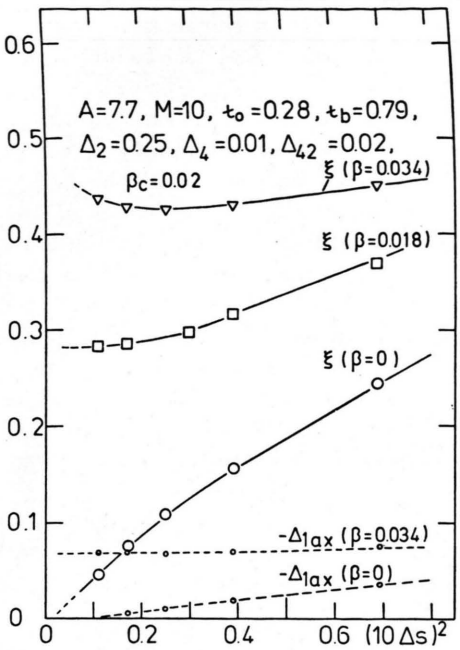

Fig. 11. Convergence of shift and helical $l=1$ corrugation Δ_{1ax} of the magnetic axis in an $l=2,4$ stellarator. The finest grid is NS/NU/NV = 30/60/60.

in $l=2$ configurations the shear reduces the axis displacement not by one order of magnitude but by a small amount. In contrast to results from asymptotic theories [3] an estimate of the maximum equilibrium β_e-value is of the order $\beta_c = 2\iota_0^2/A = 0.02$ and not of the order $2\iota_b^2/A = 0.16$. In fact, from Fig. 11 it is found that the maximum equilibrium β_e-value is $\beta_e \approx 0.03$ (if the admissible shift is bounded to $\xi \approx 0.5$); this value is somewhat higher than the estimate $\beta_c = 0.02$.

In Fig. 12 these numerical results on the axis displacement are compared with analytical results derived by Shafranov ([1], p. 130) for $l=2$ stellarators under the conditions $1/A \ll 1$, $M/A \ll 1$ (hence $\beta_b \approx \beta_c[1+(M/A)^2/2+\cdots]^2 \approx \beta_c$ for $l=2$ configurations):

$$\delta_{Sh} = \frac{\beta_c}{3\beta}\{-1+[1+3(\beta/\beta_c)^2]^{1/2}\}$$

$$\approx \frac{\beta}{2\beta_b}[1-3\beta/4\beta_b+\cdots] \qquad (10)$$

(dashed curve in the left graph of Figure 12). In leading order in β the displacement is linearly proportional to β/β_b (solid curve in the left graph

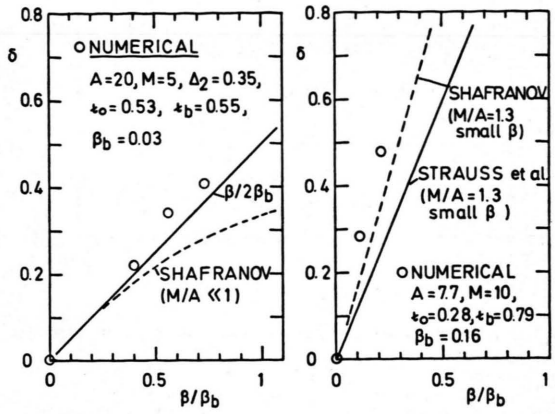

Fig. 12. Extrapolated values of the axis displacement versus β/β_b in $l=2$ (left picture) and $l=1$, 2 (right picture) stellarators compared with asymptotic theories.

of Fig. 12) and agrees well with the numerical result for the slender $l=2$ configuration.

Recently, Strauss et al. [17] calculated the displacement including leading order terms due to the finite helical aspect ratio:

$$\delta_{SM} = (\beta/2\beta_b)[1+(M/A)^2/2]^2/[1+(M/A)^2/4] \qquad (11)$$

which corresponds in leading order to (10) by neglecting terms of order $(M/A)^2$. (The factor $[1+(M/A)^2/2]^2$ also appears in Shafranov's formula including next order terms.) A graph of (11) is shown in Fig. 12 for $M/A=1.3$ (solid line in the right picture; the dashed straight is Shafranov's result $(\beta/2\beta_b)[1+(M/A)^2/2]^2$ including next order terms in (M/A)). It is found that the axis displacement obtained numerically (a) depends distinctly on the helical aspect ratio A/M, (b) agrees with results of [1, 17] in leading order in β for small values of β and M/A; hence the numerically determined axis displacement scales in the helical aspect ratio similarly to that of [1, 17] for small values of M/A and similarly to that of [1] for large values of M/A. The deviations in Fig. 12 between the numerical and the analytical results may be due to the fact that the asymptotic theories are beyond their applicability for these parameters.

3.4. *Helical $l=1$ Deformation of Magnetic Axis for Various $l=2$ Equilibria*

Simultaneously with the displacement due to the finite beta, a helical $l=1$ deformation of the plasma appears (see Figure 5). The extrapolated values

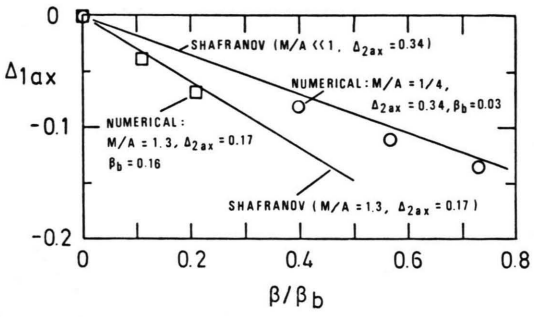

Fig. 13. Extrapolated values of the helical $l=1$ axis deformation Δ_{1ax} in small and high shear $l=2$ stellarators.

($\Delta s \to 0$) of the $l=1$ deformation Δ_{1ax} of the magnetic axis are plotted in Fig. 13 as a function of β/β_b for (a) the W VII-A stellarator with small shear (circle), (b) the short pitch $l=2, 4$ stellarator discussed above (squares), and (c) are compared with asymptotic theories. From the analytical theory by Shafranov et al. [15], taking into account leading order terms in β and Δ_{2ax}, it follows for Δ_{1ax} that

$$\begin{aligned}
&\Delta_{1ax}(\beta) - \Delta_{1ax}(\beta = 0) \\
&\approx (\beta/2\beta_c)\,\Delta_{2ax}(1 - \Delta_{2ax}^2)/(1 + \Delta_{2ax}^2) \\
&\approx (\beta/2\beta_c)\,\Delta_{2ax} + O(\Delta_{2ax}^2) \approx \delta \cdot \Delta_{2ax} \\
&\approx \frac{\beta}{2\beta_b}\,[1 + (M/A)^2/2]^2 \Delta_{2ax}\,. \qquad (12)
\end{aligned}$$

In this ordering the helical deformation Δ_{1ax} is a linear function of β and of Δ_{2ax}, and is proportional to the displacement δ. Figure 13 shows that for $l=2$ stellarators all values of the helical deformation Δ_{1ax} are close to the Shafranov curve, (12), (solid straights in the figure). Consequently, for W VII-A parameters ($M/A=1/4$, $\Delta_{2ax}=0.34$) the helical $l=1$ deformation of the magnetic axis is about 1/3 of the axis displacement.

The approximately linear dependence of both the $l=1$ deformation Δ_{1ax} and the displacement δ on β has also been found numerically in $l=1, 2$ and $l=0, 1, 2, 3$ configurations, as can be seen from Figs. 8 and 16. At sizable β-values the phase of the $l=1$ deformation of the magnetic axis may be opposite to that of the boundary.

4. Configurations with $l = 0, 1, 2, 3$ Fields

Results on a particular $l=0, 1, 2, 3$ configuration are reported here which qualitatively simulates Advanced Stellarator equilibria as reviewed in [14]. The study was also partly motivated by the result reported in Refs. [22—26] on the relation between the negative $\mathscr{V}''$ property and the reduced axis shift.

The magnetic surface contours of an equilibrium with sizable shear are shown in Fig. 14 ($\beta=0.15$ corresponds to $\langle\beta\rangle=0.04$ because of the rather peaked pressure profile). The parameters of the configuration and the dependence of the axis shift on the mesh size Δs is shown in Figure 15. The corrugations corresponding to $l=0, 1, 2, 3$ fields all have sizable amplitudes. The twist number is approximated according to (6) by $\iota = M\iota_P = 0.4 + 0.5R^2$; the value for $\beta_c = 2\iota_0^2/A = 0.032$ is rather small. Nevertheless the permissible β-value for an equilibrium with almost no axis shift is about

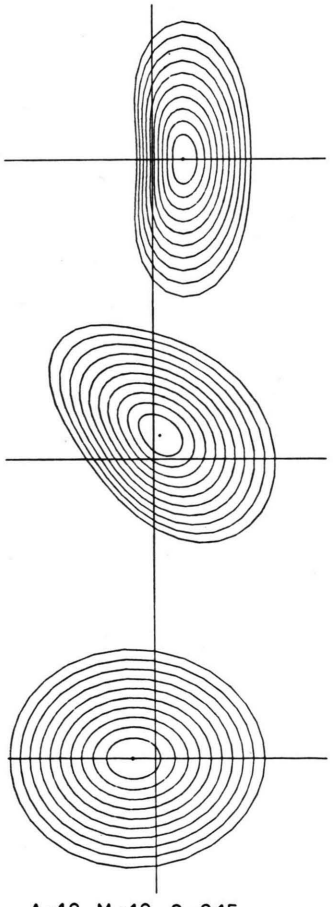

Fig. 14. Contours of magnetic surfaces of an $l=0, 1, 2, 3$ configuration: $A=10$, $M=10$, $\iota_0=0.4$, $\iota_b=0.9$, $\beta=0.15$ (corresponding $\langle\beta\rangle=0.04$), $\Delta_0=0.1$, $\Delta_{10}=0.1$, $\Delta_1=0.28$, $\Delta_{20}=-0.06$, $\Delta_2=0.23$, $\Delta_{22}=-0.08$, $\Delta_{30}=0.01$, $\Delta_3=-0.02$, $\Delta_{33}=-0.02$.

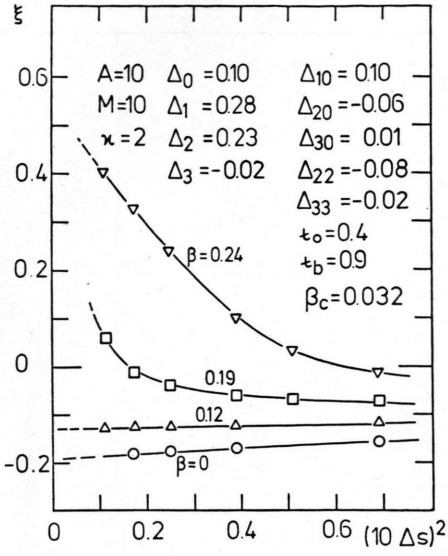

Fig. 15. Convergence of axis shift in an $l=0, 1, 2, 3$ configuration of large shear. The finest grid is NS/NU/NV = 30/60/60.

$\beta=0.15$ (corresponding to $\langle\beta\rangle=0.04$) and consequently a factor of about five higher than the above estimate for the critical β_c-value. The displacement of the plasma column is almost independent of beta in the range of $\beta \lesssim 0.12$, as can be seen in Figure 16. The helical excursions of the wall and the magnetic axis are almost the same. Hence this high shear $l=0, 1, 2, 3$ configuration is characterized by a higher magnetic stiffness as compared to the small shear and the high shear $l=2$ stellarators.

If the β-value is increased to $\beta=0.19$, the shift ξ increases nonlinearly with decreasing mesh size such that no extrapolation to zero mesh size could

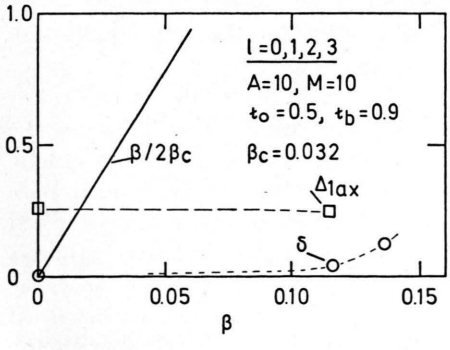

Fig. 16. Extrapolated values of the axis displacement δ and the helical $l=1$ axis deformation Δ_{1ax} versus β in $l=0, 1, 2, 3$ equilibria (same parameters as in Figure 15).

be performed. This singular behaviour could be an indication of instability (e.g. unstable rigid motion of the plasma in the radial outward direction) and of non-existence of an acceptable equilibrium. When the β-value is increased further, the extrapolation of the axis shift to zero mesh size can be performed; but the magnetic axis is very close to the wall and hence these configurations are of no interest. It has not yet been investigated whether the singular behaviour of the axis shift in this intermediate β-range is a hint for bifurcation or is akin to that found by Greene et al. [2], who showed that at a certain β-value an equilibrium does not exist in their asymptotic theory.

The results of the present study are that (a) in the case $\beta=0$ the magnetic axis is shifted in radial inward direction with respect to the geometric centre of the wall, (b) an almost centred equilibrium is obtained at $\beta=0.13$ ($\langle\beta\rangle=0.033$) (in contrast to pure $l=2$ stellarator equilibria where centred equilibria could not be found) (c) the axis displacement is rather small for $\beta \lesssim 0.12$, and (d) a positive value $\Delta_0>0$ shifts the plasma in radial inward direction. The extrapolated values of the axis displacement δ and the helical axis deformation Δ_{1ax} are shown in Fig. 16 as functions of β.

A similar mechanism of producing toroidal stellarator equilibria was used in high-beta stellarator experiments [10, 11] which are characterized by a large aspect ratio.

5. Simulation of the W VII-AS Configuration

The contours of the magnetic surfaces of the W-VII-AS configuration as taken as initial and boundary values for the BBG code are shown in Fig. 17 (left column); the vacuum field configuration computed by a field-line-tracing code as given in [27] is practically identical. The right column of Fig. 17 shows the magnetic surface contours as obtained by the BBG code for $\beta=0.045$ ($p=p_0[1-R^2]^2$, $\iota=0.38(1+0.008R^2)$, $A=9$, $M=5$, $\langle\beta\rangle=\beta/3$, $\beta_b=0.03$). As can be seen from this figure, the axis shift at $v=0$ (standing ellipse) is about half the minor half-axis. A larger shift than this value does not seem acceptable in this particular configuration. Hence the critical equilibrium beta value at the magnetic axis is about $\beta_e=0.045$. The extrapolated values of the axis shift are shown in Fig. 18 as a function of β.

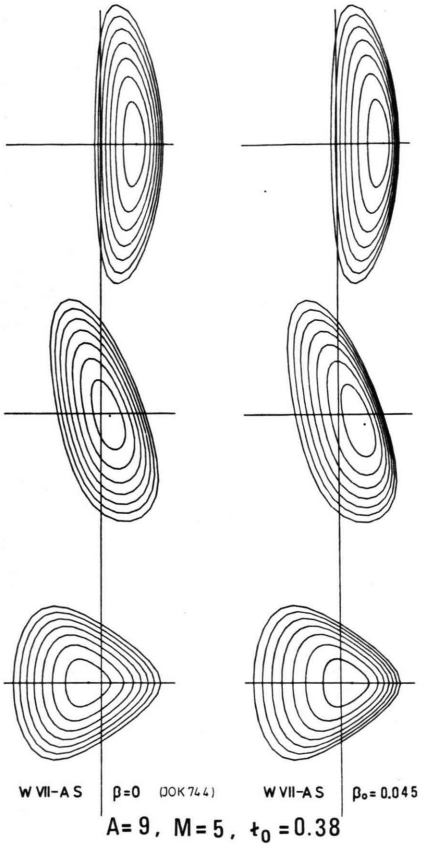

Fig. 17. Simulation of the *W* VII-AS configuration: left column for $\beta = 0$, right column for $\beta = 0.045$ ($\langle\beta\rangle = 0.015$), pressure profile $p = p_0(1 - R^2)^2$, $\iota = 0.38(1 + 0.008\ R^2)$, $\beta_c = 0.032$, $A = 9$, $M = 5$, $\Delta_0 = -0.09$, $\Delta_1 = 0.3$, $\Delta_{20} = 0.35$ $\Delta_2 \equiv \Delta_{21} = 0.29$, $\Delta_{22} = -0.02$, $\Delta_{23} = 0.04$, $\Delta_{30} = -0.06$, $\Delta_3 \equiv \Delta_{31} = 0.03$, $\Delta_{32} = -0.03$, $\Delta_{41} = 0.01$, $\Delta_{42} = -0.01$, $\delta_1 = 0$, where the boundary is given by

$$r_b(u, v)/b = (1 - \Delta_0 \cos V) \cos U + \Delta_1 \cos V - \sum \Delta_{lm} \cos[(l-1)U - mV)],$$

$$z_b(u, v)/b = (1 - \Delta_0 \cos V) \sin U + \delta_1 \sin V + \sum \Delta_{lm} \sin[(l-1)U - mV)].$$

In order to display by a finite mesh size the shift of the plasma column according to the extrapolated curve of Fig. 18, a somewhat higher β-value has been used such that the axis shift has got the extrapolated value $\xi = 0.35$.

Although the optimization of the *W* VII-AS stellarator was strongly limited by accounting for the hardware restrictions imposed by the existing *W* VII machine, the improvement in the accessible equilibrium beta is a factor of about two.

6. Conclusions

Toroidal non-symmetric solutions of the magnetohydrostatic boundary-value problem were computed with the BBG code. Since expansion in a small parameter is not applied in the code, the results are valid for arbitrary β and arbitrary finite deformations of the magnetic surfaces and of the magnetic axis. Detailed numerical convergence studies with respect to the mesh size turned out to be indispensable.

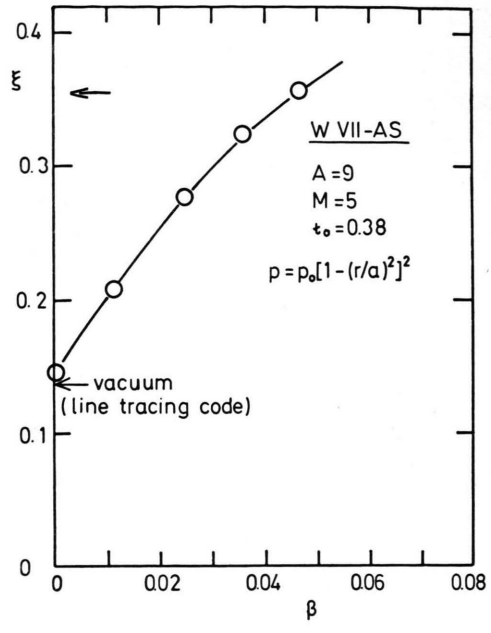

Fig. 18. Extrapolated values of the axis shift versus β for the *W* VII-AS configuration (the parameters are given in Figure 17).

It has been shown that not only in the $l = 2$ stellarator with almost no shear but also in the short pitch $l = 2$ stellarator with large shear, acceptable equilibrium beta values are not accessible for moderate values of ι. Consequently advanced stellarator configurations of moderate aspect ratio have to be discussed to increase the equilibrium beta to reasonable values.

In advanced $l = 0, 1, 2, 3$ stellarator configurations with reduced Pfirsch-Schlüter currents the radially outward displacement of the magnetic axis is a factor of at least three smaller than in pure $l = 2$ stellarators. The finite-β calculations showed that these configurations have a magnetic stiffness much higher than in pure $l = 2$ stellarators. Hence the critical equilibrium-β_e value can be increased by at least a factor of three compared with the pure $l = 2$ stellarator. The *W* VII-AS stellarator is a step in this direction.

Acknowledgements

The author is grateful to Prof. A. Schlüter and Dr. J. Nührenberg for their continued interest, stimulating discussions and criticism, and to Prof. P. Garabedian and Dr. O. Betancourt for making possible the use of their code.

[1] L. S. Solov'ev and V. D. Shafranov, Rev. Plasma Physics, Vol. 5, Consultants Bureau, New York 1970, M. A. Leontovich (Ed.). — A. I. Morozov and L. S. Solov'ev, Rev. Plasma Physics, Vol. 2.
[2] J. M. Greene, J. L. Johnson, and K. E. Weimer, Plasma Phys. 8, 145 (1966).
[3] I. S. Danilkin, Sov. J. Plasma Phys. **4**, 576 (1978).
[4] H. Grad and H. Weitzner, Phys. Fluids **12**, 1725 (1969).
[5] M. I. Mikhailov, Sov. J. Plasma Phys. **6**, 25 (1980).
[6] D. Lortz and J. Nührenberg, Theor. Comput. Plasma Physics (3rd Int. "Kiev" Conf. on Plasma Theory, IAEA-SMR-32/4, Trieste, 1977), p. 305, IAEA, Vienna 1978.
[7] F. Bauer, O. Betancourt, and P. Garabedian, A Computational Method in Plasma Physiscs, Springer-Verlag, New York 1978.
[8] R. Chodura, A. Schlüter, M. Kaufmann, and W. Lotz, Plasma Physics and Controlled Nuclear Fusion Research (Proc. 7th Int. Conf., Innsbruck 1978), Vol. 2, IAEA, Vienna 1979, p. 335. — R. Chodura and A. Schlüter, J. Comput. Phys. **41**, 68 (1981).
[9] Ch. Davis and D. Potter, Plasma Physics and Controlled Nuclear Fusion Research (Proc. 8th Int. Conf., Brussels, 1980) Vol. 1, IAEA, Vienna 1981, p. 247.
[10] E. Fünfer, M. Kaufmann, J. Neuhauser, and G. Schramm, 7th Europ. Conf. Contr. Fusion and Plasma Physics, Vol. 2, p. 151, Lausanne 1975.
[11] F. Herrnegger, O. Betancourt, and P. Garabedian, Plasma Physics and Controlled Nuclear Fusion Research (Proc. 7th Int. Conf. Innsbruck, 1978), Vol. 2, IAEA, Vienna 1979, p. 355.
[12] F. Herrnegger, Bull. Amer. Phys. Soc. **26**, 1044 (1981).
[13] R. Chodura, W. Dommaschk, F. Herrnegger, W. Lotz, J. Nührenberg, and A. Schlüter, Proc. of USA-Japan Theory Workshop on 3D MHD Studies for Toroidal Devices, p. 51, Oct. 1981, Oak Ridge, Tennessy.
[14] R. Chodura, W. Dommaschk, F. Herrnegger, W. Lotz, J. Nührenberg, and A. Schlüter, IEEE Trans. Plasma Science PS-9 (1981), p. 221.
[15] V. D. Shafranov and E. I. Yurchenko, Nucl. Fusion 8, 329 (1968).
[16] L. E. Zakharov and V. D. Shafranov, Plasma Physics and Controlled Nuclear Fusion Research (Proc. 6th Int. Conf., Berchtesgaden 1976) Vol. 2, IAEA, Vienna 1977, p. 155.
[17] H. R. Strauss and D. A. Monticello, Phys. Fluids **24**, 1148 (1981).
[18] F. Bauer, O. Betancourt, and P. Garabedian, Phys. Fluids **24**, 48 (1981).
[19] A. Schlüter and U. Schwenn, Computer Phys. Comm. **24**, 263 (1981).
[20] W. N. G. Hitchon and P. J. Fielding, Nucl. Fusion **21**, 775 (1981).
[21] D. Lortz and J. Nührenberg, Nucl. Fusion **17**, 125 (1977).
[22] J. M. Greene and J. L. Johnson, Phys. Fluids **4**, 875 (1961).
[23] W VII-A Team and W. Lotz, 9th Europ. Conf. Contr. Fusion and Plasma Physics, Vol. 1, p. 76, Oxford 1979.
[24] N. A. Manzyuk, V. I. Pyatov, A. M. Rozhkov, and V. P. Sebko, Sov. J. Plasma Phys. **3**, 7 (1977).
[25] A. Mohri and M. Azumi, J. Phys. Soc. Japan **29**, 1580 (1970). — A. Mohri, J. Phys. Soc. Japan **28**, 1549 (1970).
[26] A. A. Shishkin, Nucl. Fusion **16**, 706 (1976). — M. I. Mikhailov and V. D. Shafranov, 10th Europ. Conf. Contr. Fusion and Plasma Physics, Vol. 1, p. E-9, Moscow 1981.
[27] U. Brossmann, W. Dommaschk, F. Herrnegger, G. Grieger, J. Kisslinger, W. Lotz, J. Nührenberg, F. Rau, H. Renner, H. Ringler, J. Sapper, A. Schlüter, and H. Wobig, Concept of an Advanced Stellarator, Plasma Physics and Controlled Nuclear Fusion Research (Proc. 9th Int. Conf., Baltimore 1982).